Acta Astronautica Vol. 26, No. 11, pp. 779–798, 1992
Printed in Great Britain

0094-5765/92 $5.00 + 0.00
Pergamon Press Ltd

MATHEMATICAL MODELLING OF THE UNIFIED BIPROPELLANT PROPULSION SYSTEM†

V. SHANKAR, K. ANANTHA RAM and A. E. MUTHUNAYAGAM
Research Development, Spacecraft Propulsion System Group, Liquid Propulsion Systems Centre, Indian Space Research Organization, HAL III Stage, Bangalore 560038, India

(Received 11 April 1989; revised version received 4 December 1991)

Abstract—Present day 1.8 tonne class geosynchronous satellites carry on-board the unified bipropellant propulsion system for apogee manoeuvre, attitude and orbit control and station keeping applications. Basically the mass is expelled from the satellite for the control purposes. Hence there is a certain propellant flow rate leading to the ullage volume variations in the propellant tanks as the engines are firing. There are ullage and wall temperature variations as well. There is expansion of the pressurant in the pressurant tank with the resultant changes in the pressurant and the pressurant tank wall temperatures. The mathematical formulation of these thermodynamic processes leads to a twelve parameter initial value problem which is solved using the Runge–Kutta computer code. Real gas effects of the pressurant at high pressures are taken into account by means of the compressibility factor. The change in the temperature of the pressurant due to the throttling process in the pressure regulator is considered by means of the Joule–Kelvin coefficients. The pressure drops in the feed lines and the components are taken into account to compute the propellant supply pressures at the engine valve inlets. In the regulated mode of operation the liquid apogee motor plus a maximum of four reaction control system thrusters firing simultaneously could be handled by the model. The blowdown performance characteristics are also predicted. A computer program in FORTRAN is developed and the results as applicable to the unified bipropellant propulsion system for a 1.8 tonne class geosynchronous communication satellite are presented and discussed.

1. INTRODUCTION

Satellites in geosynchronous orbit find extensive use in long distance telecommunications, radio, T.V. programme distribution, meteorological earth observation and data relay. The propulsion system, in conjunction with other satellite subsystems, is required to perform apogee velocity manoeuvre and maintain attitude with orbit control when the satellite is in the 3-axis stabilized mode. A unified bipropellant propulsion system employing MON-3 (mixed oxides of nitrogen) and MMH (monomethyl hydrazine) propellant combination caters to propulsion requirements of such satellites and the details as applicable to INSAT II (Indian National Satellite) are given in [1]. 22.0 N thrusters provide impulse for all attitude control requirements while a 440.0 N LAM (liquid apogee motor) provides impulse for the orbital manoeuvres. The functionally redundant RCS (reaction control system) thrusters are manifolded into a single propellant storage system, such that all propellants can be fed to the functionally redundant thrusters in the event of a single thruster failure in a branch.

The thruster configuration is indicated in Fig. 1. Normally, 12 thrusters are adequate (e.g. EUTELSAT, DFS). In order to have a back-up thruster option in case of LAM failure two axial thrusters are desirable (e.g. TVSAT). Again incorporating the axial thrusters in main (BLOCK I) and redundant (BLOCK II) blocks 16 thruster configuration is selected for INSAT-II.

A schematic of the propulsion system is shown in Fig. 2. The propulsion system operates in a pressure regulated mode until the last LAM firing, after which time the pressurant source itself is isolated from the propellant storage assembly. This operation is carried by ground command (close) of the pressurant latch valve in the pressurant line. The system then operates in a blowdown mode until the completion of its useful life. The LAM is permanently isolated from the propellant supply system after the last apogee manoeuvre using pyrotechnic valve. This operation is carried out by ground command (close) of the normally open pyro valves in the oxidizer and fuel lines just upstream of the LAM. The propellant budget estimates are detailed in [2] and for Shuttle and Ariane launchers these are given in Tables 1 and 2 respectively. Manoeuvres required to be performed by the propulsion system are also indicated with specific impulse requirements as well.

The feasibility of simple bipropellant blowdown system is illustrated in [3]. Bipropellant pressurization concepts for spacecraft are evaluated by Hearn [4]. Thermodynamic considerations and concerns for bipropellant blowdown system are presented by Hearn [5]. Pasley [6] has tried to optimize stored pressurant supply for the liquid propulsion system. Estey *et al.* [7] have predicted propellant tank pressure history using state space methods. Estey's analysis resulted in a set of coupled, non-linear differential equations for the thermodynamic state variables and

†In order to avoid any further delay, this paper has been published without authors' corrections.

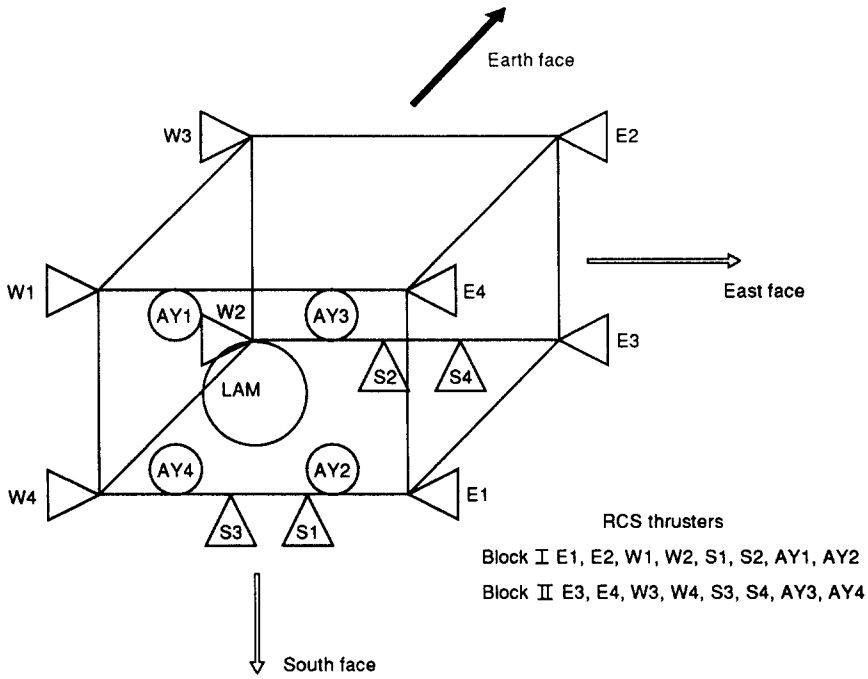

Fig. 1. Thruster configuration.

the integration is done as an initial value problem. Basically the analysis is applied to a turbo-pump system. Ricciardi *et al.* [8] have predicted the performance and the thermodynamic conditions of a bipropellant propulsion system during its life time. It is indicated that a computer program is developed and a finite difference method is used to solve the differential equations.

In this paper mathematical modelling of unified bipropellant propulsion system is carried out in six parts:

—Development of a thermodynamic model for the pressurant tank;
—Development of a thermodynamic model for the throttling process in the pressure regulator;
—Development of a thermodynamic model for the oxidizer tank;
—Development of a thermodynamic model for the fuel tank;
—Performance prediction in the regulated mode of operation; and
—Performance prediction in the blowdown mode of operation.

The feed line geometrical characteristics, the loading thermodynamic conditions in the tank and the design characteristics of the thrusters are the basis for the development of the models. Thermodynamic models for the pressurant and propellant tanks resulted in a set of twelve parameter initial value problem. The solution is obtained using Runge–Kutta computer code [9]. A computer program is developed in FORTRAN and run in UNIVAC 1100/70 system and thus the propulsion system is characterized by means of these models.

2. MATHEMATICAL MODEL

A simplified propulsion system schematic as shown in Fig. 3 is considered for the analysis. This consists of one pressurant tank, one oxidizer tank, one fuel tank, LAM and a maximum of four RCS thrusters. The propulsion system essentially consists of two parts: pressurant gas and propellent. The former consists of a pressurant tank in which the helium is stored at high pressure. The pressurant gas reaches the propellant tanks at reduced pressure via a pressure regulator which is situated along its path. In this way the pressure in the propellant remains constant so as to assure a constant pressure supply during LAM firing. The propellant part consists of two lines; one for the oxidizer and the other for the fuel both of which are somewhat similar to each other and feed both LAM and RCS thrusters. Decrease in the pressure occurs along the feeding lines due to friction on the piping walls and the pressure drop in components and these are required to be taken into account.

2.1. *Thermodynamic model for the pressurant tank*

The thermodynamic model of the pressurant tank is based on the following considerations:

(a) The external surface of the pressurant tank is assumed to be adiabatic since the ground testing is done with well insulated tanks and in orbit, the tank wall temperature changes during operation are envisaged to be small relative to the initial equilibrium temperature.
(b) The pressurant tank is assumed to be in thermal equilibrium with the pressurant; the driving temperature difference between the gas and the tank

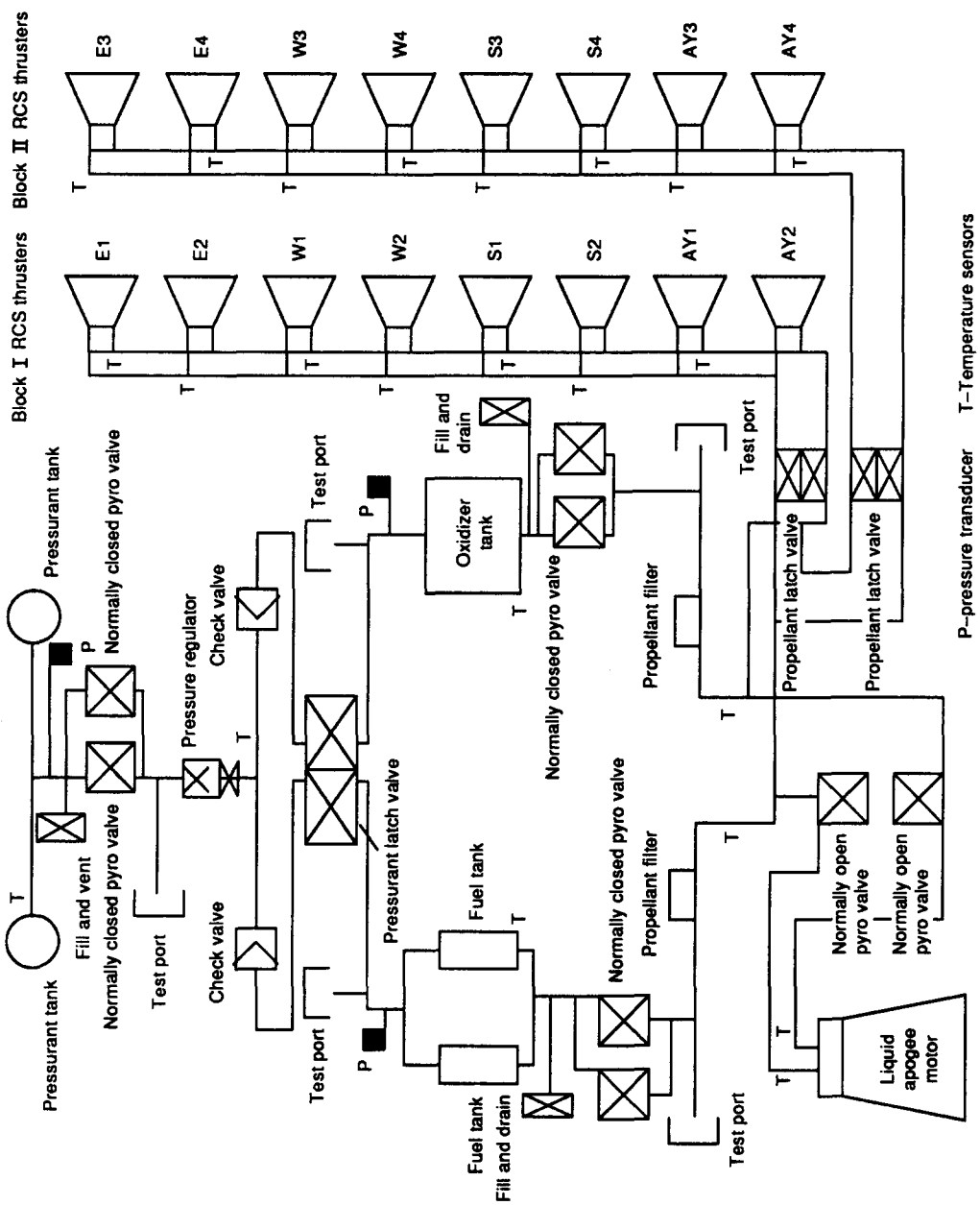

Fig. 2. Propulsion schematic.

Table 1. Propellant budget estimate (STS launch), 1887 kg lift-off mass [2]

Manoeuvre	Specific impulse *Isp* (Ns/kg)	Mass change (kg)	Mass final (kg)
Active nutation		1.5	1885.5
Despin		3.5	1882.0
Attitude hold I (pre LAM firing)		3.0	1879.0
Attitude hold II (pre LAM firing)		2.0	1877.0
LAM firing	3041.4	844.801	1032.199
Attitude hold during LAM firing	2746.8	8.184	1024.015
Attitude holding		1.5	1022.515
Transfer orbit dispersion correction	3041.4	16.674	
LAM dispersion correction	2795.85	16.06	
Dispersion correction RSS		23.15	999.365
Station acquisition	2795.85	7.123	992.241
Repositioning	2795.85	2.835	989.406
Attitude maintenance		8.5	980.906
Attitude reacquisition		1.5	979.406
North–South station keeping	2795.85	115.244	864.163
East–West station keeping	2795.85	6.532	857.631
Deorbiting	2746.8	3.117	854.514
Residual propellant		15.0	839.514
Margin		8.091	831.423
Dry mass	831.423 kg		
Total propellant required	1055.577 kg		
LAM propellant			
Oxidizer	531.531 kg		
Fuel	318.793 kg		
Propellant required for manoeuvres	205.195 kg		

is zero; this makes zero heat transfer coefficient initially.

(c) Temperature and/or pressure dependent fluid properties are required. Investigating the property variations of helium over the expected pressure and temperature ranges, it could be observed that the variation of specific heat is $<1\%$. Hence, constant specific heat hypothesis is applicable.

(d) Non-ideal behaviour of the helium at high pressure is accounted for by the use of the compressibility factor which is taken to vary with pressure alone since its variation with temperature is of the second order [10].

2.1.1. Governing equations. The control volume is the pressurant tank and the energy equation can be written as:†

$$Mh_h \delta u = \delta Q w_h - PhVs_h \delta Mh_h \quad (1)$$

where Mh_h, Ph, Vs_h are the mass, pressure and specific volume respectively of the pressurant gas in the volume, δMH_h, δU are the mass and internal energy changes during the time interval dt and $\delta Q w_h$ is the heat energy exchanged with wall during the same interval.

Applying

(a) the constant specific heat hypothesis,

(b) taking into account the compressibility factor and

(c) considering the heat exchange due to convective transfer eqn (1) becomes

$$Mh_h Cv_h (\mathrm{d}Th_h/\mathrm{d}t) = hw_h Aw_h (Tw_h - Th_h) - ZRhTh_h (\mathrm{d}Mh/\mathrm{d}t). \quad (2)$$

This equation links the change in temperature of helium due to its mass change and time.

2.1.2. Determination of the heat transfer coefficient. The determination of the heat transfer coefficient is the key to the development of a general set of equations which can be used to describe the pressurant behaviour under varying environments. Infinite heat transfer coefficient would result in a design which does not provide adequate pressurant. On the other hand zero heat transfer coefficient would increase the pressurant gas and tank weight. Although data on free convective heat transfer to a gas in a sphere are unavailable, there exists a relationship derived from the results of experiments in free convective heat transfer from the surface of a sphere to a fluid filling the interior [11]. Alcohol, glycol and water were used as fluids and a range of 3×10^8–5×10^{11} of the product GrPr was covered. The equation is

$$\mathrm{Nu} = 0.098(\mathrm{GrPr})^{0.345}. \quad (3)$$

Since the Grashof number is directly dependent on the gravity field g, the reduced heat transfer resulting from decrease in convective fluid flow at low accelerations is accounted for in the results. This fact makes the equations applicable during the variable accelerations which accompany the various spacecraft manoeuvres.

2.1.3. Heat flux from the pressurant tank wall to the pressurant. Temperature Tw_h varies with time and insulated wall assumption enables us to write the equation as

$$Mw_h Cw_h \, \mathrm{d}Th_h/\mathrm{d}t = hw_h Aw_h (Tw_h - Th_h). \quad (4)$$

2.1.4. Determination of helium flow rate. The helium flow rate is obtained by considering that the gas

†The nomenclature is given in Appendix 1 at the end of the paper.

Table 2. Propellant budget estimate (Ariane launch), 1685 kg lift-off mass [2]

Manoeuvre	Specific impulse, *Isp* (Ns/kg)	Mass change (kg)	Mass final (kg)
Attitude hold I (pre LAM firing)		3.0	1682.0
Attitude hold II (pre LAM firing)		2.0	1680.0
LAM firing	3041.4	657.61	1022.39
Attitude hold during LAM firing	2746.8	6.371	1016.019
Attitude holding		1.5	1014.519
Transfer orbit dispersion correction	3041.4	6.65	
LAM dispersion correction	2795.85	16.092	
Dispersion correction RSS		17.412	997.167
Station acquisition	2795.85	7.107	990.0
Repositioning	2795.85	2.829	987.171
Attitude maintenance		8.5	978.671
Attitude acquisition		1.5	977.171
North–South station keeping	2795.85	114.981	862.191
East–West station keeping	2795.85	6.517	855.674
Deorbiting	2746.8	3.109	852.564
Residual propellant		15.0	837.564
Margin		6.833	830.732
Dry mass	830.372 kg		
Total propellant	854.628 kg		
LAM propellant			
Oxidizer	413.755 kg		
Fuel	248.155 kg		
Propellant required for manoeuvres	192.314 kg		

in the propellant tanks consists of partial pressures of propellant vapour and helium. The pressurant flow rate is a function of propellant flow rate and can be expressed as

$$dMh_h/dt = [Po/(Rh_o Tu_o)]\dot{m}o/\rho o + [Pf/(Rh_f Tu_f)]\dot{m}f/\rho f \quad (5)$$

where Po, Pf are the total pressures in the tank, i.e.

$$Po = Ph_o + Pv_o \quad (6)$$

$$Pf = Ph_f + Pv_f. \quad (7)$$

Thus, the thermodynamic model of the pressurant tank is reduced to an initial value problem.

2.2. *Consideration of control volume between pressurant tank and propellant tank*

There is a pressurant module in between the pressurant and the propellant tanks. This module consists of pyro valves (normally closed), pressure regulator and check valves and there are tubings interconnecting these components and feed the pressurant from the pressurant tank to the propellant tanks.

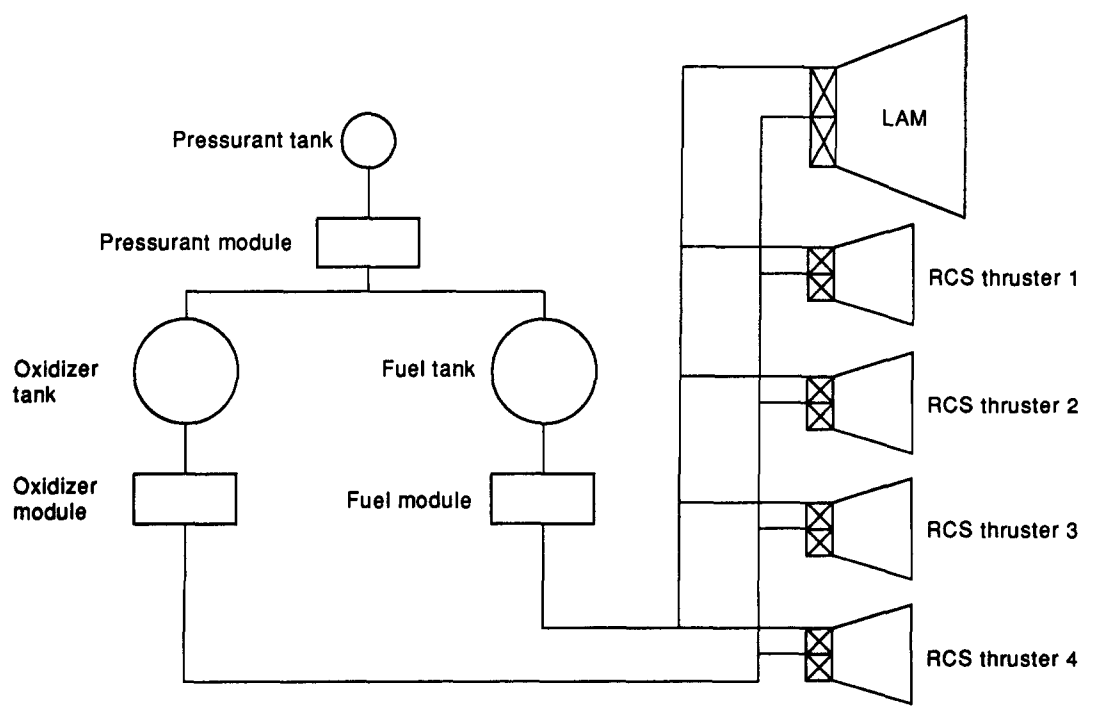

Fig. 3. Simplified propulsion system schematic.

2.2.1. Thermodynamic model of the throttling process in the pressure regulator. The pressurant gas leaving the tank flows in the gas line and passes through the pyro valve and the pressure regulator which reduces its pressure substantially.

Consider the pressurant pipe used in the propulsion system [Fig. 4(a)]. It is thermally insulated. The regulator provides a constriction to the flow of the gas. A continuous stream of gas flows through the constriction. The presence of the constriction results in a pressure difference being maintained across this constriction. Thus, the gas pressure $P1$ is greater than the gas pressure $P2$. Let $T1$ denote the temperature of the gas before the constriction and it is important to know the gas temperature $T2$ on the flow stream after the constriction.

Analysing the situation as detailed by Reif [12], let us focus attention on the system consisting of the mass M of gas lying between the dashed planes A and B shown in Fig. 4(b) and (c). Let us suppose that the planes A and B are chosen at such a distance that the volume occupied by the constriction itself is negligible compared to the volume contained between A and B. At initial time, plane B coincides with the constriction and virtually the entire mass M of gas lies towards inlet side of the constriction as in Fig. 4(b). Then it occupies some volume $V1$ corresponding to the pressure $P1$. As this mass M of gas flows down the pipe, planes A and B which define its geometrical boundaries also shift downstream of the pipe. After some time has elapsed plane A will have moved so as to coincide with the constriction and virtually the entire mass M of the gas will lie to the downstream of the constriction. There it occupies a different volume $V2$ corresponding to the lower pressure $P2$. This is the final situation illustrated in Fig. 4(c).

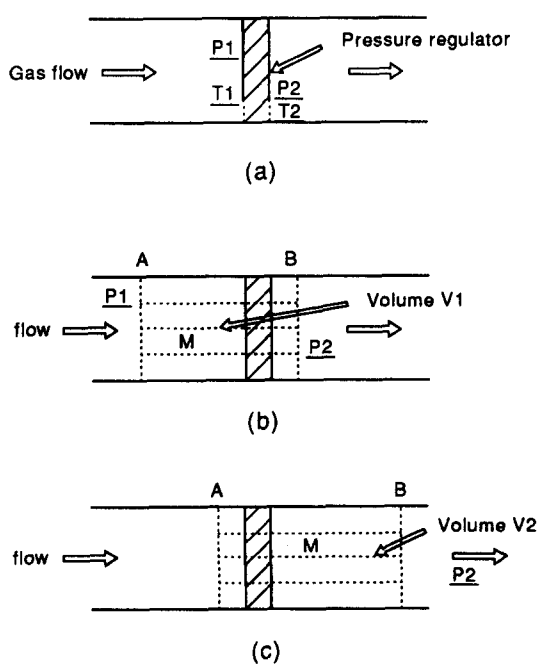

Fig. 4. (a) Steady state throttling process in which the pressurant is flowing through the regulator. (b) Diagram showing a mass M of gas passing through the regulator before passing through the constriction. (c) Diagram showing a mass M of gas passing through the regulator after passing through the constriction.

In the process just described the difference in internal energy of the mass M of gas between the final situation when it is towards the downstream and initial situation when it is to the upstream of the constriction can be expressed as

$$\Delta E = E2 - E1 = E(T2, P2) - E(T1, P1). \quad (8)$$

In this process mass M of the gas also does work. Indeed it does work $P2V2$ in displacing the gas to the downstream of the constriction by the volume $V2$ against the constant pressure $P2$. Furthermore, the gas on upstream of the constriction does work $P1V1$ on the mass M of gas by displacing it by the volume $V1$ with a constant pressure $P1$. Hence, the net work done by the mass M of gas in the process is

$$W = P2V2 - P1V1. \quad (9)$$

But no heat is absorbed by the mass M of gas in the process described. This is not just because the walls are adiabatically insulated so that no heat enters from the outside; more importantly after the steady state situation has been established, there is no temperature difference between the walls and the adjacent gas so that no heat flows from the walls into the gas. Thus,

$$Q = 0. \quad (10)$$

Application of the first law of thermodynamics to the mass M of gas yields then for the process under consideration the relation

$$\Delta E + W = Q = 0. \quad (11)$$

By eqns (9) and (10), this becomes

$$E2 - E1 + (P2V2 - P1V1) = 0$$

or

$$E2 + P2V2 = E1 + P1V1. \quad (12)$$

As

$$H = E + PV \quad (13)$$

$$H2 = H1$$

or

$$H(T2, P2) = H(T1, P1). \quad (14)$$

Thus, we can arrive at the result that in a throttling process the gas passes through the regulator in such a way that the enthalpy remains constant. It should be noted here that the passage of the gas through the constriction involves complicated irreversible non-equilibrium processes. Equilibrium situation prevails only upstream and downstream of the constriction. But a knowledge of the enthalpy function $H(T, P)$ characteristic of equilibrium macrostate of the system is sufficient to predict the outcome of the process. From a knowledge of $H(T, P)$ one can construct

curves of T vs P for various fixed values of the enthalpy H. On such a plot the initial value $T1$ and $P1$ determine a particular enthalpy curve. By virtue of eqn (14) one must end up somewhere onthis same curve as a result of the throttling process. The final temperature $T2$ can then be read off immediately from this curve for any value of the final pressure $P2$. A significant parameter in this context is the slope of these curves

$$\alpha = (\partial T/\partial P)_H \tag{15}$$

called the Joule–Kelvin coefficient. This quantity gives the change of temperature produced in a throttling process involving on infinitesimal pressure differential. Typical values of α for helium throttling as given in Zemansky [13] are

Temperature (°C)	Joule–Kelvin coefficient (deg/atm)
25	−0.0624
0	−0.0616
−100	−0.0584

Since Joule–Kelvin coefficients are negative it could be observed that the helium temperatures increase due to the throttling process. These data are used in the computer program to predict the temperature downstream of the regulator. Thus, the pressurant enters the propellant tank at a higher temperature than the temperature at the pressurant tank outlet due to the helium throttling process in the regulator.

2.3. *Thermodynamic models for oxidizer and fuel tank*

A sketch of a propellant tank and contents is shown in Fig. 5. A sphere is shown and in the case of a cylindrical tank in an actual system, a sphere of equal volumetric capacity is considered for the analysis. Propellant management device (PMD) (surface tension/screen device) ensures liquid presence at the outlet of the tanks for various manoeuvres. During LAM firing, the liquid is removed at a constant rate and consequently the gas mixture does work on the liquid as the mixture volume increases. The pressurant enters the tank at a constant pressure. In addition there is an exchange of mass and energy through the boundaries of the film layer but it is assumed that the work done by the gas mixture is transmitted directly to the liquid. Throughout the LAM firing various heat transfer processes also occur. The proposed thermodynamic model accounts for all the significant physical processes. In Fig. 5, four control columns are shown; one enveloping the mixture of pressurant gas and propellant vapour, another surrounding the liquid, the third is the film layer which is a control volume of infinitesimal thickness at the liquid and gas/vapour mixture interface and the fourth the tank itself.

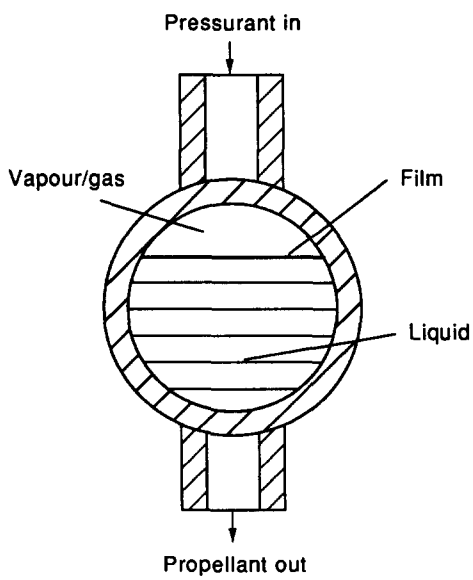

Fig. 5. Sketch of a propellant tank showing control volumes.

The following assumptions are made:

—The propellant vapour and pressurant gas are ideal gases with constant specific heats.

—The liquid has constant density and enthalpy of vapourization.

2.3.1. Governing equations. Taking the control volume 1 and applying the equation of conservation of energy

$$\delta Qw_o + \delta Ql_o - \delta W_o + hh_{en}\,dMh_o + hv_o\,dMv_o = d(Mh_o Uh_o + Mv_o Uv_o). \tag{16}$$

Since the film layer is of infinitesimal thickness [7] it is neglected. Because of perfect gas assumption eqn (16) can be written as

$$\delta Qw_o + \delta Ql_o - \delta W_o + hh_{en}\,dMh_o + Rv_o Tu_o\,dMv_o = Cp_h Tu_o\,dMh_o + (Mh_o Cp_h + Mv_o Cv_h)\,dTu_o. \tag{17}$$

It is assumed that the liquid propellent contained in the tank does not undergo temperature changes and this is acceptable if one considers propellant high thermal capacity in comparison to the heat exchanged.

2.3.1.1. Heat exchanged with the wall. The amount of heat exchanged with the tank wall is given as

$$\delta Qw_o = hw_o Au_o(Tw_o - Tu_o)\,dt. \tag{18}$$

The convective heat transfer coefficient is obtained using eqn (3). The heat transfer area referred to in eqn (18) is indeed time varying. For computational convenience the area of the ullage/wall interface (which does not include the film layer area) is correlated to the gas/vapour volume and nondimensionalized by the tank volume for a spherical tank as [7]

$$Au_o/(Vt_o)^{2/3} = 4.0675(Vu_o/Vt_o)^{0.6237}. \tag{19}$$

Temperature of the tank wall varies with time and assuming the tank is isolated from its surroundings, the temperature change is given by

$$dTw_o Mw_o(Au_o/At_o)Cw_o = hw_o Au_o(Tw_o - Tu_o)\,dt. \tag{20}$$

2.3.1.2. Heat exchanged with the propellant liquid surface. This is given as

$$\delta Ql_o = hl_o Al_o (Tl_o - Tu_o)\,dt. \quad (21)$$

For the heat transfer from the propellant to the gas/vapour mixture, a relationship developed for the upper surface of a heated plate is used [14]

$$Nu = 0.14(GrPr)^{0.333}. \quad (22)$$

The liquid surface area is calculated using the following formula [7]

$$Al_o/(Vt_o)^{2/3} = [Au_o/(Vt_o)^{2/3}] - 3.4211(Vu_o/Vt_o)^{1.2475}. \quad (23)$$

2.3.1.3. Work done by the gas/vapour mixture. Work done by the gas/vapour mixture on the liquid propellant can be considered as expansion work

$$w_o = Po\,dVu_o \quad (24)$$

and enthalpy of the gas entering

$$hh_{en} = Cp_h Th_o. \quad (25)$$

2.3.1.4. Mass of the gas and vapour in the ullage. The vapour pressure Pv_o remains constant since it is assumed that the ullage is always vapour saturated and that temperature of the liquid propellant is always constant. Differentiating gas and vapour perfect gas equations, one gets

$$dMh_o = Mh_o[(dVu_o/Vu_o) - (dTu_o/Tu_o)] \quad (26)$$

$$dMv_o = Mv_o[(dVu_o/Vu_o) - (dTu_o/Tu_o)]. \quad (27)$$

2.3.1.5. Final energy equation. Substituting eqns (18)–(27) in eqn (17) and simplifying, the final energy equation can be written as

$$dQw_o/dt + dQl_o/dt - W_o\,dVu_o/dt + hh_{en}\,dMh_o/dt + hv_o\,dMv_o/dt = Cp_h Tu_o\,dMh_o/dt + (dTu_o/dt)(Mh_o Cp_h + Mv_o Cp_v). \quad (28)$$

2.3.1.6. Governing equation for change in ullage volume. The change of tank ullage volume is a function of the change in liquid propellant volume. The ullage volume is given by

$$Vu_o = Vt_o + Vl_o. \quad (29)$$

Differentiating

$$dVu_o = -dVl_o = dMl_o/\rho_o + dMv_o/\rho_o. \quad (30)$$

Substituting the value of dMv_o given by eqn (27), one gets

$$dVu_o/Vu_o = [dMl_o/(Vu_o\rho_o - Mv_o)] - [Mv_o/(Vu_o\rho_o - Mv_o)]\,dTu_o/Tu_o. \quad (31)$$

2.3.1.7. Governing equations for fuel tank. In eqns (16)–(31) subscript o is used to refer to the oxidizer tank. Using subscript f similar equations are applicable to the fuel tank.

2.3.2. Initial value problem. The governing equations formulated based on thermodynamic models of propellant tanks constitute initial value problem. The variables are:

—oxidizer tank ullage volume
—oxidizer tank ullage temperature
—oxidizer tank wall temperature
—fuel tank ullage volume
—fuel tank ullage temperature
—fuel tank wall temperature
—helium mass in oxidizer tank
—propellant vapour mass in oxidizer tank
—helium mass in fuel tank
—propellant vapour mass in fuel tank.

Already variables, helium temperature in the pressurant tank and pressurant tank wall temperature have been accounted in the governing equations detailed in the thermodynamic model of pressurant tank. There are twelve ordinary differential equations which are implicitly related. This set of first order nonlinear differential equations is integrated numerically as an initial value problem and solved simultaneously using Runge–Kutta computer code [9].

Initial values are obtained from loading conditions. Once the loading of the propellant and pressurant gas is completed the following information is obtained:

—mass of propellant
—temperature and pressure in the propellant tank
—temperature and pressure in the pressurant tank.

Using these data, other conditions in the tanks could be obtained. For instance, the propellant density could be obtained by means of the following empirical equations [8]

$$\rho_o = 2066.0 - 1.979To \quad (32)$$

$$\rho_f = 1150.0 - 0.9395Tf. \quad (33)$$

The propellant vapour pressures in the tank ullages are evaluated by means of

$$Pv_o = 702.85423 \exp[16.519085 - (4074.693/To)] \quad (34)$$

$$Pv_f = 702.85423 \exp[15.415071 - (4599.191/Tf)]. \quad (35)$$

The volume occupied by the liquid oxidizer is determined by bearing in mind that the total oxidizer mass is given by

$$Ml_o = Vl_o\rho_o + (Vt_o - Vl_o)Pv_o/(Rv_o To). \quad (36)$$

Therefore,

$$Vl_o = [Ml_o - (Pv_o Vt_o/(Rv_o To))]/[\rho_o - (Pv_o/(Rv_o To))]. \quad (37)$$

Similarly, the fuel volume is calculated as

$$Vl_f = [Ml_f - (Pv_f Vt_f/(Rv_f Tf))]/[\rho_f - (Pv_f/(Rv_f Tf))]. \quad (38)$$

Oxidizer tank ullage is given by

$$Vu_o = Vt_o - Vl_o. \tag{39}$$

Fuel tank ullage is given by

$$Vu_f = Vt_f - Vl_f. \tag{40}$$

Partial pressure of the pressurant in the ullage is given by

$$Ph_o = Po - Pv_o \text{ for oxidizer} \tag{41}$$

$$Ph_f = Pf - Pv_f \text{ for fuel} \tag{42}$$

and mass of this gas in the tank ullage is given by

$$Mh_o = Ph_o Vu_o/(RhTo) \text{ for oxidizer} \tag{43}$$

$$Mh_f = Ph_f Vu_f/(RhTf) \text{ for fuel.} \tag{44}$$

The pressurant gas mass which is dissolved in the liquid propellant can be estimated by empirical equations [8]

$$Mhl_o = Ph_o Ml_o 3.335 \times 10^{-11}(To/294.0)^2 \tag{45}$$

$$Mhl_f = Ph_f Ml_f 2.059 \times 10^{-11}(Tf/294.0)^2. \tag{46}$$

In this way all the thermodynamic considerations at the beginning of the mission are known and are used as initial conditions.

2.4. Thruster performance prediction during regulated mode

Usually LAM plus a few RCS thrusters are fired to take the spacecraft from transfer orbit to geostationary orbit. The model is able to predict the performance as a function of time for LAM plus a maximum of four RCS thrusters working simultaneously. The model is supplied with feed line geometry in terms of number of Tee's, Ell's, length and size of tubing used and maximum pressure drop across various components. The following design characteristics of LAM and RCS thrusters must be supplied to the model:

—thrust
—flow rate
—mixture ratio
—nozzle throat area
—nozzle area ratio
—combustion chamber pressure
—oxidizer supply pressure
—fuel supply pressure.

These design values are used in the first step of the iterative process which aims at determining the true mass flow and true thrust.

2.4.1. Computation of equivalent discharge coefficient. Expressions for calculating the equivalent discharge coefficients are given below:

$$Cdo_i = \dot{m}o_i/\sqrt{(Pso_i - Pc_i)\rho o_i} \text{ for oxidizer} \tag{47}$$

$$Cdf_i = \dot{m}f_i/\sqrt{(Psf_i - Pc_i)\rho f_i} \text{ for fuel.} \tag{48}$$

2.4.2. Computation of flow rate in feed line. By using the first tentative mass flow rate in primary lines (a primary line is that which directly feeds one engine) the mass flow rates in the secondary lines (a secondary line is that which is between two primary lines) can be determined by means of the following equations for oxidizer and fuel:

$$\begin{aligned}
\dot{m}so_1 &= \dot{m}o_1 + \dot{m}o_2 + \dot{m}o_3 + \dot{m}o_4 + \dot{m}o_5 \\
\dot{m}so_2 &= \dot{m}s_1 - \dot{m}o_1 \\
\dot{m}so_3 &= \dot{m}so_2 - \dot{m}o_2 \\
\dot{m}so_4 &= \dot{m}so_3 - \dot{m}o_3 \\
\dot{m}so_5 &= \dot{m}so_4 - \dot{m}o_4 \\
\dot{m}sf_1 &= \dot{m}f_1 + \dot{m}f_2 + \dot{m}f_3 + \dot{m}f_4 + \dot{m}f_5 \\
\dot{m}sf_2 &= \dot{m}sf_1 - \dot{m}f_1 \\
\dot{m}sf_3 &= \dot{m}sf_2 - \dot{m}f_2 \\
\dot{m}sf_4 &= \dot{m}sf_3 - \dot{m}f_3 \\
\dot{m}sf_5 &= \dot{m}sf_4 - \dot{m}f_4.
\end{aligned} \tag{49}$$

2.4.3. Computation of pressure drop and propellant supply pressures. At this point it is necessary to calculate the propellant supply pressure by calculating the pressure drop in the lines and feed components. There is an oxidizer module in between the oxidizer tank and thruster. This oxidizer module consists of a pyro valve (normally open, for LAM only) and a latch valve (for RCS thruster only). The fuel module between the fuel tank and thrusters consists of similar components. The propellant supply pressures are evaluated using Bernoulli's equation as follows:

$$\begin{aligned}
Pso_i &= Po - \Delta P_{PMD} - \Delta P_{PV} - \Delta P_F - \Delta P_{PV} \\
&\quad - \sum [f(l/d)vs_o^2 \rho o/2g] \text{ for LAM}
\end{aligned} \tag{50}$$

$$\begin{aligned}
&= Po - \Delta P_{PMD} - \Delta P_{PV} - \Delta P_F - \Delta P_{LV} \\
&\quad - \sum [f(l/d)vs_o^2 \rho o/2g] \text{ for RCS thrusters}
\end{aligned} \tag{51}$$

$$\begin{aligned}
Psf_i &= Pf - \Delta P_{PMD} - \Delta P_{PV} - \Delta P_F - \Delta P_{PV} \\
&\quad - \sum [f(l/d)vs_f^2 \rho f/2g] \text{ for LAM}
\end{aligned} \tag{52}$$

$$\begin{aligned}
&= Pf - \Delta P_{PMD} - \Delta P_{PV} - \Delta P_F - \Delta P_{LV} \\
&\quad - \sum [f(l/d)vs_f^2 \rho f/2g] \text{ for RCS thrusters.}
\end{aligned} \tag{53}$$

Velocity is determined using the first tentative mass flow rate

$$vs_o = \dot{m}so/(\rho o A s_o) \tag{54}$$

and

$$vs_f = \dot{m}so/(\rho f A s_f). \tag{55}$$

The friction coefficient is calculated based on the Reynolds number. Pressure drops in Tee's, Ell's, sudden contraction, sudden expansion etc. are converted to equivalent length of the tube by means of nomogram given in [15]. A subroutine calculates the pressure drop values and the supply pressures at the thruster valve inlets.

2.4.4. Governing flow rate equation. It is possible to write the flow rate equation as

$$Ath_i Pc_i g/C_i^* = Cdo_i\sqrt{(Pso_i - Pc_i)\rho o} + Cdf_i\sqrt{(Psf_i - Pc_i)\rho f}. \quad (56)$$

The characteristic velocity C_i^* depends on the combustion process and essentially depends on the combustion chamber pressure and mixture ratio which is given by

$$r_i = [Cdo_i\sqrt{(Pso_i - Pc_i)\rho o}]/[Cdf_i\sqrt{(Psf_i - Pc_i)\rho f}]. \quad (57)$$

For this particular mixture ratio, equilibrium combustion gas temperature, molecular weight and γ values for the MON and MMH propellant combination are obtained by a built-in subroutine which interpolates the data given from [16]. These values have been obtained from standard equilibrium thermo-chemical calculations. The characteristic velocity is calculated as

$$C_i^* = [gRuTc_i/(M_i\gamma_i)]^{1/2}[(\gamma_i + 1)/2]^{(\gamma_i+1)/[2(\gamma_i-1)]}. \quad (58)$$

2.4.5. Solution by iterative process. Equation (56) is solved by squaring both sides to obtain a quadratic equation. The first two terms are used by expanding the square root term binomially. A subroutine gives the solution of the said quadratic equation.

The new value of combustion chamber pressure is used to determine the new mass flow rates (both oxidizer and fuel) for LAM and each RCS thruster. If the new mass flow rates differ from the value already assumed, the process is repeated using new values. The iterative process stops when the values obtained are very close to those obtained in previous step. The realized value of specific impulse is calculated as

$$Isp_i = 2Ru\gamma_i Tc_i/[g(\gamma_i - 1)\bar{M}_i] \times [1 - (Pe_i/Pc_i)^{(\gamma_i-1)/\gamma_i}]^{1/2}. \quad (59)$$

True thrust is given by

$$F_i = Ath_i Pc_i Isp_i/C_i^*. \quad (60)$$

These conditions are considered stationary for a time interval Δt (quasi-stationary).

Typically LAM firing is carried out in regulated mode for about 90 min and for each time interval the initial value problem of 12 equations is solved simultaneously and then eqns (32)–(60) are solved to predict the performance during the same time interval.

2.5. Thruster performance preidiction during the blowdown mode of operation

After LAM firing RCS thrusters are operated in blowdown mode for the remainder of the mission. This section deals with the governing equations for blowdown mode.

2.5.1. Governing equations for the blowdown mode. The propellant gas remaining in the tanks undergoes slow expansion while the propellants are being used. This model assumes that this expansion occurs in isothermal conditions. Taking this into account and using the perfect gas equations for pressurant gas and propellant vapour, we get

$$Ph_o' = Ph_o Vu_o/Vu_o' \quad (61)$$

$$Mv_o' = Mv_o Vu_o'/Vu_o. \quad (62)$$

These equations are obtained by assuming vapour pressure and ullage temperature are constants. To complete the system of equations, we add

$$Vu_o' = Vu_o + \Delta Ml_o/\rho o + (Mv_o' - Mv_o)/\rho o. \quad (63)$$

This equation gives the new ullage volume as a function of propellant mass used and new propellant vapour mass. Substituting this in eqn (62) for Mv_o', and solving for Vu_o', one gets,

$$Vu_o' = [Vu_o + (\Delta Ml_o/\rho o) - Mv_o]/[1 - (Mv_o/(\rho o Vu_o))]. \quad (64)$$

Similarly for fuel

$$Vu_f' = [Vu_f + (\Delta Ml_f/\rho f) - Mv_f]/[1 - (Mv_f/(\rho_f Vu_f))]. \quad (65)$$

Once the new ullage is determined new pressure can be calculated. In real flight, application pressure transducers record the pressures in the oxidizer and fuel lines through telemetry. Hence, the mass change corresponding to pressure change can be predicted with this model and performance of the RCS thrusters could be predicted using eqns (32)–(60).

3. RESULTS AND DISCUSSION

The mathematical model developed is applied to unified bipropellant propulsion systems typical of geostationary satellites of the early nineties. Salient data pertaining to INSAT-II unified bipropellant propulsion system are taken from [1,17–19] and are given in Appendix 2. A computer program is developed in FORTRAN and run in UNIVAC 1100/70 computer system. The results are presented and discussed below.

3.1. Results of the twelve parameter initial value problem

The thermodynamic models of the pressurant tank and propellant tanks has led to a system of twelve ordinary differential equations with initial values. These are solved using a Runge–Kutta computer code [9]. In INSAT-II application cylindrical (cylindrical shirt with spherical ends) propellant tanks are used and in this model the equivalent volume of a sphere is considered. There are two fuel tanks and two pressurant tanks in the system. Only one fuel tank and one pressurant tank are considered for the analysis. Both the tanks are taken to feed equally to the total flow requirements. The results hold good for

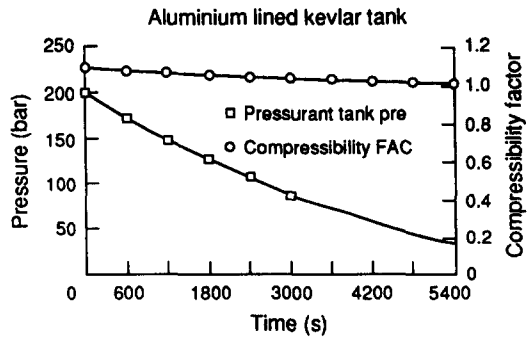

Fig. 6. Pressurant tank pressure and compressibility factor variations with time.

either of the fuel or pressurant tanks. Studies [20] on space storage of liquid propellant indicate that free convection will occur at g levels of the order of 10^{-7} for small temperature change. This is taken into account for the computation of convective heat transfer coefficient.

3.1.1. Results based on the thermodynamic model of the pressurant tank. Governing equations for the thermodynamic model of the pressurant tank require as input geometrical parameters of the pressurant tank and the corresponding pressure capabilities. The results are presented both for the baseline aluminium lined Kevlar tank and optional titanium tanks. The salient parameters are:

	Al lined Kevlar tank	Titanium tank
Volume (m^3)	0.04	0.03773
Pressure (bar)	200.0	212.0

The apogee manoeuvre is usually carried out in either of the following ways depending on the mission operations:

—3 steps with reheating during coast phase
—2 steps with most of the required impulse being provided in the first step itself.

The latter option is preferred and the propulsion system for INSAT II is designed to cater to 5400 s continuous firing. The results are presented and discussed for this case.

3.1.1.1. Pressure variations in the pressurant tank. The results are plotted in Fig. 6. It could be observed that the pressure drops from 200 to 35.52 bar in the case of aluminium lined Kevlar tank. Figure 7 indicates that the pressure drops from 212 to 16 bar in the case of titanium tank. From the pressure regulator point of view a minimum of 30 bar pressure is required in the pressurant tank. Hence, the titanium tank is not a desirable proposition where 5400 s continuous firing is envisaged, whereas an aluminium lined Kevlar tank could comfortably be used.

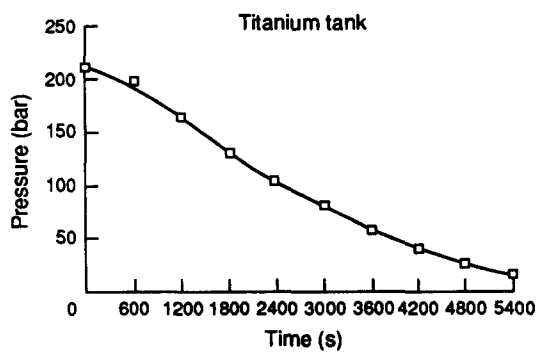

Fig. 7. Pressurant tank pressure variations with time.

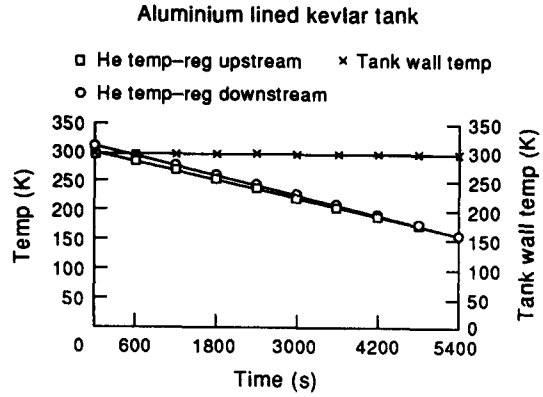

Fig. 8. Variation of helium temperature and pressurant tank wall temperature with time.

Real gas behaviour of the helium gas at high pressure is accounted by means of the compressibility factor in the analysis. Typical variation of the compressibility factor is plotted in Fig. 6. The maximum and minimum compressibility factor values are 1.0822 and 1.01467 corresponding to the pressure 200 and 35.52 bar respectively.

3.1.1.2. Temperature variations in the pressurant tank. Variations of the helium temperature are plotted in Figs 8 and 9 for aluminium lined Kevlar tank and titanium tank respectively. Temperature upstream of the pressure regulator is the same as the temperature at the pressurant tank outlet. Figure 8 indicates that the helium temperature in the pressurant tank decreases with respect to time during the process of the LAM firing. Temperature of the pressurant decreases from 298 to 157.8 K at the end

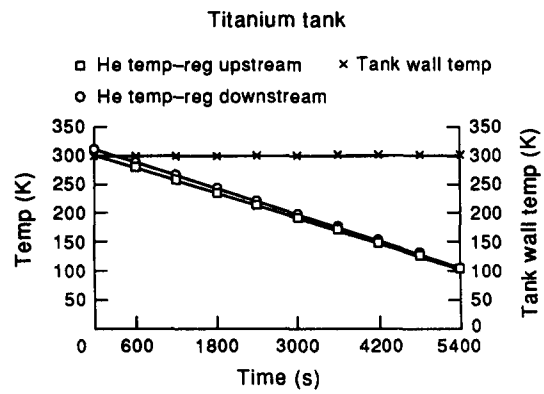

Fig. 9. Variation of helium temperature and tank wall temperature with time.

of 5400 s in the case of the aluminium lined Kevlar tank, whereas the corresponding decrease is from 298 to 104 K in the case of the titanium tank. This is due to the fact that with the outflow of gas from the pressurant tank the remaining gas will be expanded and its temperature will drop. As the heat energy exchanged with the wall is a strong function of the thermal mass of the pressurant tank and as the specific heat of aluminium is much higher than titanium there is a steep fall in temperature in the case of the titanium tank.

The pressurant tank wall temperature variations are also plotted in Figs 8 and 9 for the aluminium lined Kevlar tank and titanium tank respectively. Initially the tank walls are at a temperature of 298 K and there is a negligible variation during LAM firing operation.

3.1.2. Results based on the thermodynamic model of the throttling process in the pressure regulator. There is a temperature increase of helium due to the throttling process in the regulator. Helium temperature downstream of the regulator is plotted in Figs 8 and 9 for the aluminium lined Kevlar tank and titanium tank respectively. Helium temperature downstream of the regulator varies from 309.3 to 159 K during LAM firing in the case of the aluminium lined Kevlar tank. In the case of the titanium tank, temperature of the helium downstream of the regulator is 104.4 K at the end of LAM firing. Typical values of the maximum and minimum downstream regulator temperature increases are 11.3 and 1.2 K during the beginning and the end of LAM firing respectively. This is because at the beginning of LAM firing the pressurant enters the regulator at a high pressure whereas the pressurant enters the regulator at a reduced pressure at the end of LAM firing due to gas expansion in the tank. The regulator downstream pressure is constant. The results enable us to compute enthalpy of the pressurant gas entering the propellant tank.

3.1.3. Results based on the thermodynamic models of the propellant tanks. Ullage volume and temperature variations in the propellant tanks, propellant tank wall temperature variations with time and variations of the pressurant and propellant vapour masses in the ullage are obtained from the thermodynamic models of the propellant tanks and the results are detailed below.

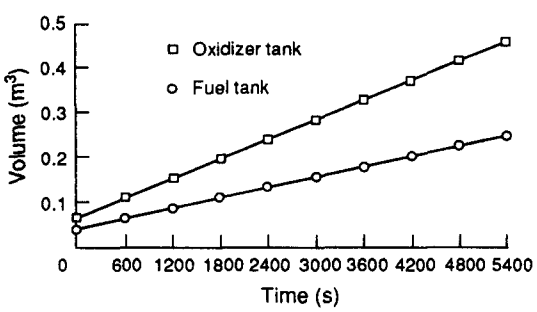

Fig. 10. Variations of ullage volume with time.

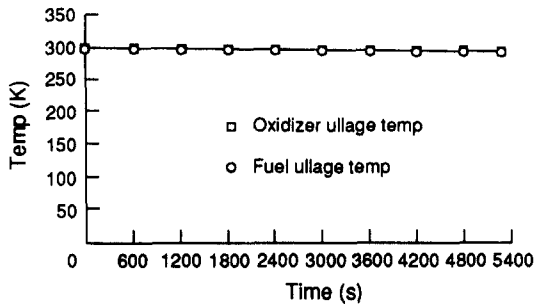

Fig. 11. Ullage temperature variation in oxidizer tank and fuel tank with time.

3.1.3.1. Ullage volume variations in the propellant tanks. As the propellants are depleted from the propellant tanks, the ullage volume should increase. These variations are plotted in Fig. 10. The initial ullage volume in the oxidizer tank is 0.0642 m^3 and it increases to 0.449049 m^3 after 5400 s LAM firing. The initial ullage volume in the fuel tank is 0.0415 m^3 and it increases to 0.239965 m^3 after 5400 s LAM firing. The ullage variations with time more or less obey a straight line law.

3.1.3.2. Ullage temperature variations in the propellant tanks. These are plotted in Fig. 11. There is a marginal decrease in the ullage temperature with time. In the case of the oxidizer tank the temperature decreases from 298 to 297.3 K at the end of LAM firing, whereas in the case of the fuel tank the temperature decreases from 298 to 297 K at the end of LAM firing.

3.1.3.3. Propellant tank wall temperature variations with time. These are plotted in Fig. 12. Initially the propellant tank walls are at 298 K and there is a negligible propellant tank wall temperature variation with time during LAM firing.

3.1.3.4. Variations of the constituent masses in the ullage of propellant tanks. The propellant tank ullage consists of helium gas and the propellant vapour. Variations of the helium mass and the oxidizer vapour mass in the oxidizer tank are plotted in Fig. 13. The initial mass of the helium in the oxidizer tank is 0.165 kg whereas the initial oxidizer vapour mass is 0.238 kg. At the end of LAM firing the helium mass is 1.16 kg whereas the oxidizer vapour mass is 1.669 kg.

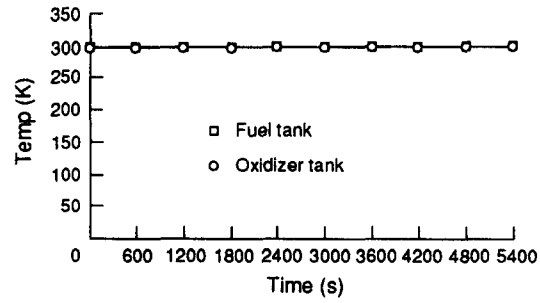

Fig. 12. Variation of propellant tank wall temperature with time.

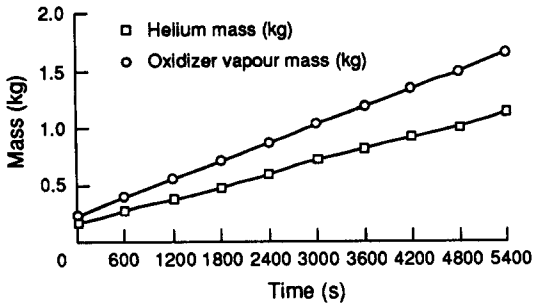

Fig. 13. Variation of helium mass and vapour mass in oxidizer tank with time.

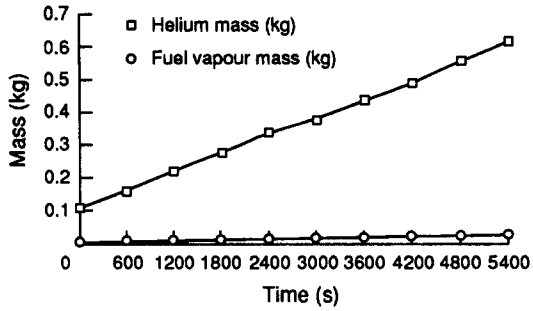

Fig. 14. Variation of helium mass and vapour mass in fuel tank with time.

Variations of the helium mass and fuel vapour mass in the fuel tank are plotted in Fig. 14. The initial helium mass is 0.107 kg whereas the initial fuel vapour mass is 0.005 kg. At the end of LAM firing the helium mass is 0.619 kg, whereas the fuel vapour mass is 0.0307 kg.

3.2. Performance of LAM and RCS thrusters during regulated mode

In this section performance data of LAM and RCS thrusters while firing in regulated mode as predicted by the mathematical model are presented. The RCS thrusters considered are AY1, AY2, AY3 and AY4. Exact locations of these thrusters and the tube lengths connecting these thrusters and LAM are taken from [19]. The required data for LAM and RCS thruster tube sizes are taken from Appendix 2. It could be observed from Tables 1 and 2 that the maximum of propellant is required in the case of the STS launch and the results are presented for about 1054 kg initial loading (Appendix 2). It could be observed from Table 1 that about 80% propellant is expended in transfer orbit manoeuvre to near circular orbit. Appendix 2 gives the maximum specified pressure drop of components at a certain oxidizer flow rate. The corresponding pressure drop for MMH and helium is evaluated based on the consideration that the pressure drop is directly proportional to density whereas it is directly proportional to the square of the flow rate.

The model takes into account LAM plus a maximum of four RCS thrusters firing simultaneously. Tables 3–7 give the performance details of LAM and RCS thrusters.

3.2.1. Propellant tank pressure during regulated mode firing. The pressure regulator downstream pressure is set to 16 bar and there is a slight drop in check valve and pressurant lines. The pressures in fuel and oxidizer tanks as a function of time are indicated in Table 3. These pressures more or less remain constant. The variation is of the order of +0.5% in the oxidizer tank and +0.43% in the fuel tank.

3.2.2. Propellant supply pressure at LAM and RCS thruster valve inlets. These are of vital importance to predict the performance. These data reflect the drop in propellant lines and components. The oxidizer line pressure drop is observed to be higher than the fuel. This is because of higher density and flow rate of the oxidizer than the fuel. Between LAM and RCS thrusters it could be observed that propellant supply pressure increases from LAM to RCS thrusters. This is because LAM lines handle the maximum of flow rates and this flow rate decreases as we go to RCS thrusters.

3.2.3. Mixture ratio. Typically, LAM oxidizer supply pressure is 15.261 bar fuel supply pressure is 15.6104 bar. This leads to a mixture ratio of 1.63845. It could be seen from Table 3 that the mixture ratio reduces to 1.60382 at 2000 s and varies slightly afterwards. It could also be observed from Table 3 that

Table 3. LAM performance during regulated mode firing

Time, *t* (s)	Propellant tank pressure, *P* (bar)		Propellant supply pressure *Ps* (bar)		Chamber pressure, *Pc* (bar)	Mixture ratio by mass, *r* (oxidizer/fuel)	Thrust, *F* (N)	Specific impulse, *Isp* (Ns/kg)	Characteristic velocity, *C** (m/s)
	Po	*Psf*	*Pso*	*Psf*					
400	15.8614	15.8775	15.261	15.6104	7.34948	1.63845	436.56	2981.757	1683.33
800	15.8704	15.8857	15.27	15.6186	7.35177	1.63845	436.7	2981.778	1683.33
1200	15.8775	15.892	15.2771	15.6249	7.35359	1.63844	436.811	2981.81	1683.33
1600	15.8848	15.8983	15.2843	15.6313	7.3554	1.63843	436.922	2981.83	1683.33
2000	15.8919	15.9046	15.2914	15.6375	7.3871	1.60382	436.921	2980.178	1689.66
2400	15.8978	15.9098	15.2974	15.6428	7.3887	1.60368	437.009	2980.168	1689.67
2800	15.9039	15.9152	15.3035	15.6481	7.3902	1.60366	437.101	2980.178	1689.67
3200	15.91	15.9206	15.3096	15.6536	7.39174	1.60365	437.194	2980.20	1689.67
3600	15.9163	15.9262	15.3159	15.6591	7.3933	1.60363	437.288	2980.21	1689.67
4000	15.9227	15.9318	15.3222	15.6647	7.39488	1.60361	437.383	2980.23	1689.68
4400	15.9288	15.9371	15.3283	15.6701	7.39641	1.60359	437.475	2980.242	1689.68
4800	15.9344	15.9421	15.334	15.6751	7.39785	1.60356	437.561	2980.25	1689.68
5200	15.9402	15.9472	15.3397	15.6802	7.39931	1.60354	437.649	2980.26	1689.68

Table 4. RCS thruster (AY1) performance during regulated mode firing along with LAM

Time, t (s)	Propellant supply pressure, Ps (bar)		Chamber pressure, Pc (bar)	Mixture ratio by mass, r (oxidizer/fuel)	Thrust, F (N)	Specific impulse, Isp (Ns/kg)	Characteristic velocity, C (m/s)
	Pso	Psf					
400	15.55952	15.6882	7.66117	1.66666	22.9981	2829.63	1673.98
800	15.6042	15.6964	7.6635	1.66666	23.4687	2829.65	1673.98
1200	15.6114	15.7026	7.66539	1.66666	23.4086	2829.68	1673.98
1600	15.6186	15.709	7.66725	1.66665	23.0169	2829.71	1673.98
2000	15.6257	15.7153	7.66966	1.66664	23.0225	2829.73	1673.99
2400	15.6316	15.7205	7.67063	1.66663	23.0273	2829.75	1673.99
2800	15.6377	15.7259	7.6722	1.66662	23.0321	2829.78	1673.99
3200	15.6439	15.7313	7.6738	1.66661	23.037	2829.80	1674.00
3600	15.6501	15.7368	7.6754	1.6666	23.042	2829.82	1674.01
4000	15.6565	15.7425	7.67704	1.66658	23.047	2829.85	1674.01
4400	15.6626	15.7478	7.67862	1.66657	23.0518	2829.87	1674.02
4800	15.6683	15.7528	7.68011	1.66655	23.0564	2829.89	1674.62
5200	15.674	15.7579	7.68163	1.66654	23.0611	2829.92	1674.03

throughout 5200 s the mixture ratio is within 1.65 ± 0.05. Likewise, the mixture ratio of RCS thruster is 1.66666. It could be observed from Tables 4–7 that the order of magnitude of variation is very small.

3.2.4. Chamber pressure and thrust. LAM chamber pressure is typically 7.34948 bar and thrust is 436.56 N. These vary to 7.39931 bar and 437.649 N at 5200 s. RCS thruster chamber pressure is typically 7.66 bar and thrust is 22.99 N. Tables 4–7 give these variations for the four RCS thrusters considered.

3.2.5. Specific impulse and characteristic velocity. LAM characteristic velocity is typically 1683.33 m/s and specific impulse is 2981.757 Ns/kg. RCS thruster characteristic velocity has a typical value of 1673.98 m/s and specific impulse of 2829.63 Ns/kg. Tables 3–7 show these small variations as a function of time.

3.3. Performance during blowdown mode

For a typical 1.8 tonne class geosynchronous satellite, the total propellant required is 1054 kg [2]. Out of the 1054 kg of loaded propellant, about 80% is consumed in the apogee manoeuvre and the remaining 20% is available for RCS thruster use in blowdown mode after leaving residual and margin. After apogee manoeuvre the pressurant part of the system is cut off by closing the pressurant latch valve and LAM also is cut off by closing normally open pyro valve. Subsequently, RCS thrusters are used in blowdown mode for attitude and inclination correction purposes. This section deals with prediction of performance of the system in blowdown mode. As the temperature effects are important the performance details are given for three different oxidizer and fuel temperatures (278, 288 and 298 K). Also temperature biasing (278 K oxidizer, 288 K fuel, 288 K oxidizer, 278 K fuel, 293 K oxidizer, 303 K fuel, 303 K oxidizer and 293 K fuel) effects are presented.

3.3.1. Pressure variations in the blowdown mode. These are plotted in Fig. 15. As the mass change increases from 20 to 180 kg the propellant tank pressure decreases from 15.7848 to 13.5573 bar for the oxidizer and 15.9573 to 13.7156 bar for fuel respectively. The propellant supply pressures are also plotted in Fig. 15. As the mass change increases from 20 to 180 kg the propellant supply pressure decreases from 15.5917 to 13.3642 bar for the oxidizer and 15.8647 to 13.609 bar for fuel respectively. It could be observed that with increase in mass change, there is a decrease in pressure and the difference between the propellant tank pressure and the propellant supply pressure gives the pressure drop in the feed line and components. These data are plotted for constant oxidizer and fuel temperatures (278 K).

3.3.2. Ullage volume variations in the blowdown mode. As the propellant is depleted the ullage volume in the propellant tank increases. These are plotted in Fig. 16. Initial oxidizer tank ullage volume is

Table 5. RCS thruster (AY2) performance during regulated mode firing along with LAM

Time, t (s)	Propellant supply pressure, Ps (bar)		Chamber pressure, Pc (bar)	Mixture ratio by mass, r (oxidizer/fuel)	Thrust, F (N)	Specific impulse, Isp (Ns/kg)	Characteristic velocity, C (m/s)
	Pso	Psf					
400	15.6295	15.6922	7.66546	1.66666	23.0114	2829.68	1673.98
800	15.6385	15.7004	7.66781	1.66666	23.0186	2829.71	1673.98
1200	15.6456	15.7067	7.66968	1.66666	23.0244	2829.73	1673.98
1600	15.6529	15.7131	7.67153	1.66665	23.0301	2829.76	1673.98
2000	15.66	15.7193	7.67335	1.66664	23.0357	2829.78	1673.99
2400	15.6659	15.7246	7.67491	1.66663	23.0405	2829.80	1673.99
2800	15.672	15.73	7.67649	1.66662	23.0454	2829.83	1673.99
3200	15.6782	15.7354	7.678	1.66661	23.0503	2829.85	1674.00
3600	15.6844	15.7409	7.67969	1.6666	23.0552	2829.87	1674.01
4000	15.6908	15.7465	7.68132	1.66658	23.0602	2829.90	1674.01
4400	15.6969	15.7519	7.6829	1.66657	23.0651	2829.92	1674.02
4800	15.7025	15.7569	7.68439	1.66655	23.0692	2829.94	1674.02
5200	15.7083	15.762	7.6859	1.66654	23.0743	2829.92	1674.03

Table 6. RCS thruster (AY3) performance during regulated mode firing along with LAM

Time, t (s)	Propellant supply pressure, Ps (bar)		Chamber pressure, Pc (bar)	Mixture ratio by mass, r (oxidizer/fuel)	Thrust, F (N)	Specific impulse Isp (Ns/kg)	Characteristic velocity, C^* (m/s)
	Pso	Psf					
400	15.6502	15.6951	7.6681	1.66666	23.0195	2829.71	1673.98
800	15.6593	15.7003	7.67041	1.66666	23.0268	2829.74	1673.98
1200	15.6664	15.7096	7.67231	1.66666	23.0326	2829.76	1673.98
1600	15.6736	15.716	7.67417	1.66665	23.0383	2829.79	1673.98
2000	15.6807	15.7223	7.67559	1.66664	23.0439	2829.81	1673.99
2400	15.6867	15.7275	7.67755	1.66663	23.0487	2829.83	1673.99
2800	15.6927	15.7329	7.67912	1.66662	23.0536	2829.86	1673.99
3200	15.6969	15.7383	7.68071	1.66661	23.0584	2829.88	1674.00
3600	15.7052	15.7438	7.68232	1.6666	23.0634	2829.90	1674.01
4000	15.7115	15.7494	7.68395	1.66658	23.0684	2829.93	1689.68
4400	15.7176	15.7548	7.68553	1.66657	23.0733	2829.95	1689.68
4800	15.7233	15.7598	7.68702	1.66655	23.0778	2829.97	1689.68
5200	15.729	15.7649	7.68854	1.66654	23.0825	2830.00	1689.68

Table 7. RCS thruster (AY4) performance during regulated mode firing along with LAM

Time, t (s)	Propellant supply pressure, Ps (bar)		Chamber pressure, Pc (bar)	Mixture ratio by mass, r (oxidizer/fuel)	Thrust, F (N)	Specific impulse Isp (Ns/kg)	Characteristic velocity, C^* (m/s)
	Pso	Psf					
400	15.6683	15.6969	7.67031	1.66666	23.0264	2829.74	1673.98
800	15.6773	15.7051	7.67265	1.66666	23.0336	2829.77	1673.98
1200	15.6845	15.7114	7.67452	1.66666	23.0394	2829.79	1673.98
1600	15.6917	15.7177	7.67638	1.66666	23.0451	2829.81	1673.98
2000	15.6988	15.724	7.67819	1.66664	23.0507	2829.84	1673.99
2400	15.7047	15.7293	7.67976	1.66663	23.0555	2829.86	1673.99
2800	15.7108	15.7346	7.68133	1.66662	23.0604	2829.88	1673.99
3200	15.717	15.74	7.68292	1.66661	23.0653	2829.9	1674.00
3600	15.7232	15.7456	7.68453	1.6666	23.0702	2829.93	1674.01
4000	15.7296	15.7512	7.68616	1.66658	23.0752	2829.95	1674.01
4400	15.7357	15.7566	7.68773	1.66657	23.0801	2829.97	1674.02
4800	15.7413	15.7616	7.68923	1.66655	23.0847	2830.00	1674.02
5200	15.471	15.7666	7.69074	1.66654	23.0893	2830.02	1674.04

0.448981 m^3 whereas the initial fuel tank ullage volume is 0.239932 m^3. These volumes increase to 0.494705 and 0.263361 m^3 for the oxidizer and fuel tanks respectively at the end of the blowdown process. The plots are for constant oxidizer and fuel temperatures (278 K).

3.3.3. Flow rate and mixture ratio variations in the blowdown mode. These are plotted in Fig. 17. The blowdown process decreases the oxidizer and fuel flow rates. As the mass change increases from 20 to 180 kg the oxidizer flow rate decreases from 4.908×10^{-3} to 4.317×10^{-3} kg/s whereas the fuel flow rate decreases from 2.947×10^{-3} to 2.625×10^{-3} kg/s. The mixture ratio by mass is maintained within 1.65 ± 0.05 as indicated in Fig. 17. The plots are constant oxidizer and fuel temperature (278 K).

3.3.4. Variations of the dissolved helium masses in the blowdown mode. The solubility of helium in each propellant is an important factor in blowdown systems and the amount of dissolved gas is calculated using empirical equations [eqns (45) and (46)]. These are plotted in Fig. 18. With an increase in mass change from 20 to 180 kg the helium mass dissolved in oxidizer decreases from 0.0075 to 0.0065 kg whereas the helium mass dissolved in the fuel decreases from 0.0027 to 0.0023 kg. During thruster operation the dissolved gas is expelled along with the propellant.

3.3.5. Chamber pressure thrust variations in the blowdown mode. During the blowdown process the chamber pressure and the thrust decrease. These are reflected in Fig. 19. As the mass change increases

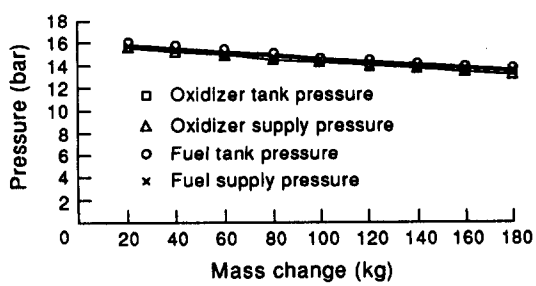

Fig. 15. Variation of pressures with mass change in blowdown mode.

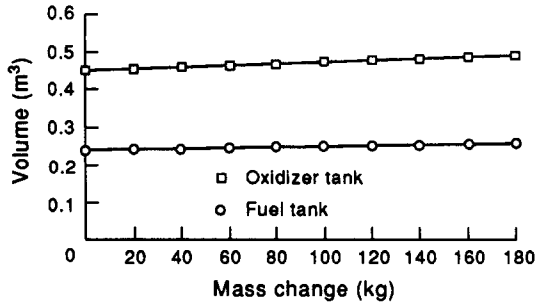

Fig. 16. Variation of ullage volume with mass change in blowdown mode.

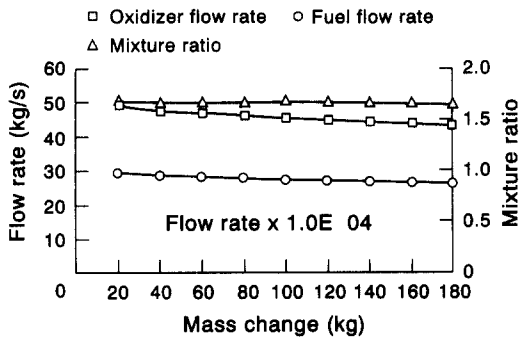

Fig. 17. Variation of flow rate and mixture ratio with mass change in blowdown mode.

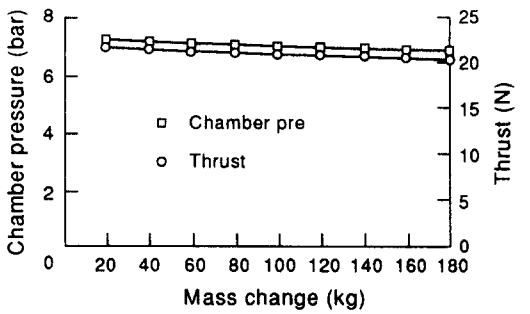

Fig. 19. Variation of chamber pressure and thrust with mass change in blowdown mode.

from 20 to 180 kg the combustion chamber pressure decreases from 7.28 to 6.84 bar whereas the thrust decreases from 21.82 to 20.4 N. These plots are for constant oxidizer and fuel temperatures (278 K).

3.3.6. Specific impulse and characteristic velocity variations in the blowdown mode. Vacuum specific impulse and characteristic velocity variations in the blowdown process are given in Fig. 20. The specific impulse is maintained at 2825.5 ± 0.5 N s/kg in the entire blowdown range. The characteristic velocity is maintained at 1678 ± 4 m/s in the entire blowdown range. These are reflected in Fig. 20. These plots are for constant oxidizer and fuel temperature (278 K).

3.3.7. Temperature effects on the RCS thrusters performance in the blowdown mode. Usually oxidizer and fuel temperatures are maintained between 278 to 303 K by spacecraft thermal management [1]. In this section effects of temperature variations in the RCS thruster performance are presented. Tables 8–10 depict the temperature effects for 60, 120 and 180 kg mass change respectively.

3.3.7.1. Constant oxidizer and fuel temperature. The results are presented for three different constant oxidizer and fuel temperatures (278, 288 and 298 K). It could be observed from Tables 8–10 that for a particular mass change and with an increase in propellant temperatures there is a decrease in

—propellant tank pressure
—propellant supply pressure
—mixture ratio
—combustion chamber pressure
—thrust
—specific impulses
—characteristic velocity.

However, the order of magnitude of the changes is small and the mixture ratio is maintained within 1.65 ± 0.05.

3.3.7.2. Temperature biasing. Temperature biasing effects are given in Tables 8–10. The following temperature biasing are considered:

—oxidizer at 278 K and fuel at 288 K
—oxidizer at 288 K and fuel at 278 K
—oxidizer at 293 K and fuel at 303 K
—oxidizer at 303 K and fuel at 293 K.

It could be observed from Tables 8–10 that increasing the oxidizer temperature compared to the fuel temperature leads to

—decrease in the oxidizer tank pressure
—increase in the fuel tank pressure
—decreases in the oxidizer supply pressure
—increase in the fuel supply pressure
—decrease in the mixture ratio
—increase in the chamber pressure
—increase in the thrust
—increase in the specific impulse
—increase in the characteristic velocity.

The mixture ratio is maintained within 1.65 ± 0.05 for all the conditions.

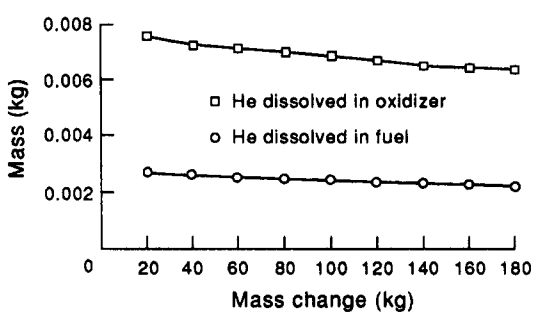

Fig. 18. Variation of dissolved helium masses with mass change in blowdown mode.

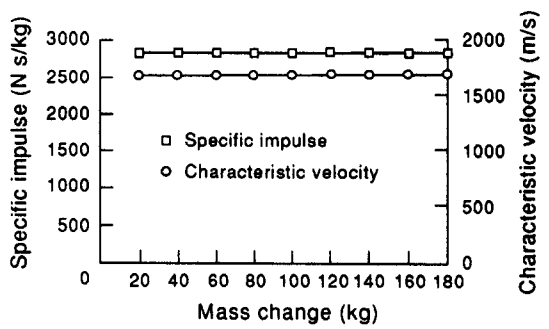

Fig. 20. Variation of specific impulse and characteristic velocity with mass change.

Table 8. RCS thruster performance during blowdown mode (mass change 60 kg)

Temperature	Propellant tank pressure, P (bar)		Propellant supply pressure, Ps (bar)		Mixture ratio by mass, r (oxidizer/fuel)	Combustion chamber pressure, Pc (bar)	Thrust, F (N)	Specific impulse, Isp (Ns/kg)	Characteristic velocity, C^* (m/s)
	Po	Pf	Pso	Psf					
Oxidizer 278 K Fuel 278 K	15.1645	15.2256	14.9714	15.1189	1.65986	7.16288	21.4411	2825.96	1676.58
Oxidizer 288 K Fuel 288 K	15.1468	15.2161	14.9554	15.1092	1.65916	7.16138	21.4348	2826.16	1676.83
Oxidizer 298 K Fuel 298 K	15.1317	15.2062	14.9383	15.0991	1.6584	7.15982	21.4282	2826.37	1677.11
Oxidizer 278 K Fuel 288 K	15.1644	15.2162	14.9713	15.1093	1.66084	7.16022	21.4351	2825.62	1676.22
Oxidizer 288 K Fuel 278 K	15.1486	15.2255	14.9554	15.1188	1.65818	7.164	21.4406	2826.42	1677.19
Oxidizer 293 K Fuel 303 K	15.1402	15.2013	14.9496	15.0939	1.65983	7.15779	21.4253	2825.91	1676.59
Oxidizer 303 K Fuel 293 K	15.1228	15.2111	14.9294	15.1041	1.65694	7.16179	21.4308	2826.82	1677.63

Table 9. RCS thruster performance during blowdown mode (mass change 120 kg)

Temperature	Propellant tank pressure, P (bar)		Propellant supply pressure, Ps (bar)		Mixture ratio by mass, r (oxidizer/fuel)	Combustion chamber pressure, Pc (bar)	Thrust, F (N)	Specific impulse, Isp (Ns/kg)	Characteristic velocity, C^* (m/s)
	Po	Pf	Pso	Psf					
Oxidizer 278 K Fuel 278 K	14.3176	14.433	14.1245	14.3264	1.65225	6.99425	20.9628	2825.91	1679.23
Oxidizer 288 K Fuel 288 K	14.2858	14.4138	14.0925	14.3069	1.65073	6.99086	20.8888	2826.21	1679.73
Oxidizer 298 K Fuel 298 K	14.2518	14.3938	14.0584	14.2866	1.64905	6.9873	20.8738	2826.53	1680.26
Oxidizer 278 K Fuel 288 K	14.3173	14.4145	14.1242	14.3076	1.65432	6.989	20.8917	2825.33	1678.53
Oxidizer 288 K Fuel 278 K	14.286	14.4323	14.0928	14. 3257	1.64865	6.99589	20.8994	2826.72	1677.38
Oxidizer 293 K Fuel 303 K	14.2688	14.3843	14.0755	14.277	1.65466	6.98367	20.8699	2825.80	1679.27
Oxidizer 303 K Fuel 293 K	14.2343	14.4032	14.0408	14.2961	1.64593	6.9907	20.8768	2827.17	1681.22

4. CONCLUSION

The unified bipropellant propulsion system has been investigated analytically. The generated models have the potential of finding applications in the ground testing and in-orbit operation of the propulsion system. The models are capable of predicting the performance of the engines during the regulated and blowdown modes of operations. The gas expansion process in the pressurant tank could be predicted and temperature changes due to the throttling process in the pressure regulator could be computed. The propellant depletion characteristics in the propellant tanks could be predicted both for the regulated and blowdown modes of operations.

Table 10. RCS thruster performance during blowdown mode (mass change 180 kg)

Temperature	Propellant tank pressure, P(bar)		Propellant supply pressure, Ps (bar)		Mixture ratio by mass, r (oxidizer/fuel)	Combustion chamber pressure, Pc (bar)	Thrust, F (N)	Specific impulse, Isp (Ns/kg)	Characteristic velocity, C^* (m/s)
	Po	Pf	Pso	Psf					
Oxidizer 278 K Fuel 278 K	13.5573	13.7156	13.3642	13.609	1.64492	6.83722	20.4017	2825.35	1681.52
Oxidizer 288 K Fuel 288 K	13.5123	13.6882	13.319	13.5813	1.64259	6.83195	20.3799	2825.64	1682.2
Oxidizer 298 K Fuel 298 K	13.4642	13.6596	13.2708	13.5524	1.64001	6.82636	20.3565	2825.92	1682.91
Oxidizer 278 K Fuel 288 K	13.5567	13.6898	13.3636	13.5829	1.64802	6.83009	20.387	2824.69	1680.58
Oxidizer 288 K Fuel 278 K	13.5128	13.7139	13.3196	13.6073	1.63949	6.83871	20.3933	2826.14	1683.05
Oxidizer 293 K Fuel 303 K	13.488	13.6466	13.2947	15.5393	1.64464	6.82184	20.3536	2825.19	1681.6
Oxidizer 303 K Fuel 293 K	13.4397	13.6722	13.2462	13.5651	1.63532	6.83036	20.3574	2826.44	1684.14

Acknowledgements—The authors gratefully acknowledge the constructive criticisms of the anonymous reviewer. Neat typing by Shri Devappa Lalgondar and drafting by Shri K. M. P. Kutty are acknowledged. The authors wish to thank ISRO Satellite Centre authorities for allocating computer time in UNIVAC 1100/70 computer.

REFERENCES

1. V. Shankar, Preliminary design review, propulsion, INSAT-II test spacecraft project. Indian Space Research Organization, Bangalore, INTS-PDR-PSN-90-01(0) (1984).
2. Y. N. Bhushan, M. G. Chandrasekhar *et al.*, Preliminary design review, mission planning and analysis, INSAT-II test spacecraft project. Indian Space Research Organization, Bangalore, INTS-PDR-MSN-01-90-01(0) (1984).
3. H. C. Hearn, Feasibility of simple bipropellant blowdown systems. *J. Spacecraft Rockets* **17,** 157–158 (1980).
4. H. C. Hearn, Evaluation of bipropellant pressurization concepts for spacecraft. *J. Spacecraft Rockets* **19,** 320–325 (1982).
5. H. C. Hearn, Thermodynamic considerations in bipropellant blowdown systems. *J. Spacecraft Rockets* **21,** 219–221 (1984).
6. G. F. Pasley, Optimization of stored pressurant supply for liquid propulsion systems. *J. Spacecraft Rockets* **7,** 1478–1480 (1970).
7. P. N. Estey, D. H. Lewis and M. Connor, Prediction of a propellant tank pressure history using state space methods. *J. Spacecraft Rockets* **20,** 49–54 (1983).
8. A. Ricciardi and E. Pergastini, Prediction of the performance and the thermodynamic conditions of a bipropellant propulsion system during its life time. *AIAA, SAE, ASME and ASEE Joint Propulsion Conference*, San Diego, Calif., AIAA Paper 87-1771 (1987).
9. G. E. Forsythe, M. A. Malcom and C. B. Moler, Initial value problems in ordinary differential equations. *Computer Methods for Mathematical Computations*, Chap. VI, pp. 110–147 (1977).
10. R. D. McCarty and R. B. Stewart, An equation of state for calculating the thermodynamic properties of helium at lower temperatures. Progress in research on thermodynamic and transport properties. Paper presented at *II Symposium on Thermophysical Properites*, The American Society of Mechanical Engineers. Academic Press, New York (1962).
11. W. H. Roudebush, An analysis of the problem of tank pressurization during outflow. NASA TND 2585 (1985).
12. R. Reif, *Fundamentals of Statistical and Thermal Physics*. McGraw–Hill, New York (1965).
13. M. W. Zemansky, *Heat and Thermodynamics*. McGraw–Hill, New York (1957).
14. J. P. Holman, *Heat Transfer*. McGraw–Hill, New York (1972).
15. C. King, *Piping Handbook*, 5th edn. McGraw–Hill, New York (1973).
16. R. J. Hoffman, W. D. English, R. G. Olding and W. T. Webber, Plume contamination effects prediction. The CONTAM Computer Program, AFRPL TR 71-109 (1971).
17. V. Shankar, Material selection for the feedlines of INSAT-II propulsion system. Liquid Propulsion Systems Center, Bangalore, LPSC/INSAT/PSN/SE/14/86.
18. V. Shankar, INSAT-II propulsion system, Technical Note. Liquid Propulsion Systems Center, Bangalore, LPSC/INSAT/PSN/SE/11/RV(1)/87.
19. V. Shankar, INSAT-II propulsion systems layout, Revision 2. Drg. No. LPSC/PSN/SE/0007(B)/87.
20. W. C. Reynolds and H. M. Satterlee, Liquid propellant behaviour at low and zero 'g'. The dynamic behaviour of liquid in a moving container. NASA Sp-106 (1966).

APPENDIX 1

Nomenclature

A = area, m^2
Al = liquid surface area, m^2
As = tubing cross-section, m^2
At = tank's internal surface area, m^2
Ath = nozzle throat area, m^2
Au = interface area between tank wall and ullage, m^2
Aw = tank wall area, m^2
Cdo = oxidizer equivalent discharge coefficient, $m^{5/2}/s$
Cdf = fuel equivalent discharge coefficient, $m^{5/2}/s$
Cp = specific heat at constant pressure, kJ/kg K
Cv = specific heat at constant volume, kJ/kg K
Cw = specific heat of tank wall material, kJ/kg K
C^* = characteristic velocity, m/s
d = tube diameter, m
E = internal energy, kJ
f = friction coefficient
F = thrust, N
g = acceleration due to gravity; 9.81 m/s^2
Gr = Grashof number, $g\beta\,\Delta\,TL^3\rho^2/\mu^2$
h = enthalpy, kJ/kg
hh = enthalpy of helium entering the propellant tank, kJ/kg
hv = enthalpy of liquid propellant vapour leaving the liquid state and entering the ullage, kJ/kg
hw = convective heat transfer coefficient (for heat exchange with the tank wall), kJ/m^2s K
hl = convective heat transfer coefficient (for heat exchange through propellant liquid surface), kJ/m^2s K
Isp = vacuum specific impulse, Ns/kg
k = thermal conductivity, kJ/ms K
l = tube length, m
L = characteristic dimension, m
m = mass flow rate, kg/s
mo = oxidizer flow rate, kg/s
mf = fuel flow rate, kg/s
mso = oxidizer flow in secondary line, kg/s
msf = fuel flow in secondary line, kg/s
M = molecular weight of combustion products, kg/kg mol
M = mass, kg
Mh = helium mass, kg
Mhl = helium mass dissolved in propellant, kg
Ml = propellant mass, kg
Mv = propellant vapour mass, kg
Mw = tank mass, kg
Nu = Nusselt number, hL/k
P = pressure, bar
Pc = chamber pressure, bar
Ph = helium pressure, bar
Po = oxidizer tank total pressure, bar
Pf = fuel tank total pressure, bar
Pe = nozzle exit plane pressure, bar
Pso = oxidizer supply pressure (at thruster value inlet), bar
Psf = fuel supply pressure (at thruster valve inlet), bar
Pt = pressurant tank pressure, bar
Pr = Prandtl number, $Cp\mu/K$
Q = heat exchanged, kJ
Qw = heat energy exchanged with the wall, kJ
Ql = heat energy exchanged with the propellant liquid surface, kJ
r = mixture ratio by mass (oxidizer to fuel)
Ru = universal gas constant, 8.31434 kJ/k mol K
R = gas constant, kJ/kg K
Rh = helium gas constant, kJ/kg K
Rv = propellant vapour gas constant, kJ/kg K
t = time, s
T = temperature, K
Tc = combustion chamber temperature, K

Th = helium temperature, K
Tl = temperature of liquid propellant, K
Tw = wall temperature, K
Tu = ullage temperature, K
Uh = internal energy of gas mass, kJ/kg
Uv = internal energy of propellant vapour mass, kJ/kg
v = velocity, m/s
V = volume, m^3
Vh = volume of helium tank, m^3
Vl = propellant volume, m^3
Vs = specific volume, m^3
Vt = tank volume, m^3
Vu = ullage volume, m^3
W = work done by gas/vapour mixture, kJ
Z = compressibility factor.

Greek

Δ = parameter change during the time interval, Δt
ρo = oxidizer density, kg/m^3
ρf = fuel density, kg/m^3
ΔP = pressure drop, bar
α = Joule–Kevlin coefficient
β = coefficient of expansion, $1/T$ for calculating Grashof number (for a perfect gas)
γ = specific heat ratio
μ = viscosity, Ns/m^2.

Subscript

en = entry to propellant tank
F = filter
f = fuel
h = helium
i = 1–5 (LAM, RCS thrusters 1–4)
LV = latch valve
o = oxidizer
PMD = propellant management device
PV = pyro valve

Superscript

' = new condition (after isothermal expansion) in blow-down mode operation
d = differential operator
δ = small change.

APPENDIX 2

Salient Data Pertaining to INSAT-II Unified Bipropellant Propulsion System [1, 17–19]

1. Pressurant tank

1.1. Aluminium lined Kevlar tank (baseline)

Shape	Near spherical
Diameter	0.44 m
Volume	0.04 m^3
Mass	11.4 kg
Maximum operating pressure	200 bar
No. on-board	2
Location	AEV (anti Earth viewing) panel top

1.2. Titanium tank (optional)

Shape	Near spherical
Diameter	0.412 m
Volume	0.03773 m^3
Mass	11.5 kg
Maximum operating pressure	212 bar
No. on-board	2
Location	AEV panel top

2. Oxidizer Tank

Shape	Cylindrical
Diameter	0.875 m
Overall length	1.155 m
Volume	0.5182 m^3
Mass	23.77 kg
Maximum operating pressure	16 bar
Pressure drop in PMD	0.08 bar
Material	Ti–6Al–4V
No. on-board	1
Location	Core of central cylinder

3. Fuel tank

Shape	Cylindrical
Diameter	0.6 m
Overall length	1.15 m
Volume	0.2685 m^3
Mass	15.86 kg
Maximum operating pressure	16 bar
Pressure drop in PMD	0.08 bar
Material	Ti–6Al–4V
No. on-board	2
Location	AEV panel top

4. Liquid apogee motor (design conditions)

Steady state thrust	440 ± 12
Propellant supply pressure at the valve inlet	
Oxidizer	15 bar
Fuel	15 bar
Propellant flow rate	
Oxidizer	0.095 kg/s
Fuel	0.058 kg/s
Mixture ratio (by mass)	1.65 ± 0.05
Specific impulse	3041.1 Ns/kg
Throat area	3.59826×10^{-4} m
Combustion chamber pressure	7 bar
Nozzle exit plane pressure	2.9 mbar
Mass	4.5 kg
No. on-board	1
Location	In the core of the central cylinder

5. Reaction control system thrusters (design conditions)

Steady state thrust	22 ± 2 N
Propellant supply pressure at the valve inlet	
Oxidizer	15 bar
Fuel	15 bar
Propellant flow rate	
Oxidizer	0.005 kg/s
Fuel	0.003 kg/s
Mixture ratio (by mass)	1.65 ± 0.05
Specific impulse	2795.85 Ns/kg
Throat area	1.1181029×10^{-4} m^2
Combustion chamber pressure	7 bar
Nozzle exit plane pressure	4 mbar
Mass	0.9 kg
No. on-board	16 (grouped into two batches of eight)
Location	10 Thrusters (W1, W4, E4, E1, AY1, AY2, AY3, AY4, S1, S3) on AEV panel
	6 Thrusters (W3, W2, E2, E3, S2, S4) on EV (Earth viewing) panel

6. Pressure regulator

Upstream pressure	200–24 bar
Downstream pressure	16 bar
Regulation band	± 0.5 bar
Mass	0.95 kg
No. on-board	1
Location	AEV top

7. Check valve

Maximum operating pressure	16 bar
Pressure drop (at 0.2×10^{-3} kg/s of helium flow rate)	0.4 bar
Mass	0.20 kg
No. on-board	2
Location	AEV top

8. Pyro valves (normally closed)

Maximum operating pressure	200 bar
Pressure drop (at 0.105 kg/s of flow rate of MON-3)	0.1 bar
Mass	0.15 kg
No. on-board	6
Location	AEV top

9. Pyro valves (normally open)

Maximum operating pressure	16 bar
Pressure drop (at 0.095 kg/s of flow rate of MON-3)	0.1 bar
Mass	0.15 kg
No. on-board	2
Location	AEV top

10. Latch valve

Maximum operating pressure	16 bar
Pressure drop (at 0.047 kg/s of flow rate of MON-3)	
Mass	0.31 kg
No. on-board	6
Location	AEV top
Baseline	Single valve
Option	Bipropellant valve (pressure drop 0.34 bar at 0.136 kg/s of MON-3)

11. Fill and drain valve and test ports

Maximum operating pressure	200 bar
Mass	0.15 kg
No. on-board	
Fill and drain	2
Fill and vent	1
Test ports	5

12. Filters

	Absolute μm	Nominal μm
System filter	40	20
Pyro valve	No built-in filter	
Pressure regulator	15	2
Check valves	No built-in filter	
Latch value (Optional)		
Pressurant latching valve	25	10
Propellant latching valves	40	20
Oxidizer and fuel valves	40	20
Fill and drain valves	No filters	
System filter pressure drop (at 0.12 kg/s flow rate of MON-3)	0.1 bar	

13. Tubing

Pressurant part	
Outer diameter	0.006 m
Inner diameter	0.0046 m
Propellant part	
LAM	
Outer diameter	0.01 m
Inner diameter	0.0087 m
RCS thrusters	
Outer diameter	0.006 m
Inner diameter	0.0046 m

14. Pressure transducers

High pressure transducer range	0–300 bar
Low pressure transducer range	0–30 bar
No. of high pressure transducer	1
No. of low pressure transducers	2
Mass	0.1 kg

15. Propellants

	MON-3	MMH
Composition		
MMH (% by weight)	—	98.3 max
Water equivalent (% by weight)	0.05 max	1.5 max
Particulate (mg/l)	10 max	10 max
NO (% by weight)	2.5–3.0	—
$N_2O_4 + NO$ (% by weight)	99.5 max	—
Chloride content (% by weight)	0.04 max	
Iron content (ppm)	0.2 max	
Normal boiling point (K)	294.6	360.0
Freezing point (K)	262.0	222.0
Critical temperature (K)	431.0	594.0
Critical pressure (bar)	101.38	82.41
Vapour specific heat at film temperature (kJ/kg K)	1.248	4.165
Liquid specific heat at 300 K	1.5072	2.888
Vapour molecular weight (kg/kg mol)	46.008	46.074
Latent heat of vapourization at normal boiling point (kJ/kg)	414.49	879.228
Liquid thermal conductivity (W/mK)	0.128	0.228
Viscosity at 300 K (Ns/m^2)	0.000446	0.00104
Density at 300 K (kg/m^3)	1450.0	880.0
Vapour pressure (bar)	0.958 at 293 K	0.069 at 300 K
	4.130 at 327 K	6.900 at 420 K
Surface tension at 300 K (N/m)	0.28 $\times 10^{-5}$	0.47 $\times 10^{-5}$

16. Loading conditions (envisaged)

Oxidizer	656 kg
Fuel, kg	398 kg
Pressurant tank pressure	200 bar
Oxidizer tank pressure	16 bar
Fuel tank pressure	16 bar
Temperature	
Helium	298 K
Oxidizer	298 K
Fuel	298 K
Initial wall temperature	298 K